Applied Catalysis B: Environmental 324 (2023) 122277

Contents lists available at ScienceDirect

Applied Catalysis B: Environmental

journal homepage: www.elsevier.com/locate/apcatb

Synergetic roles of pyridinic nitrogen and carbonyl sites in nitrogen-doped carbon for the metal-free transfer hydrogenation reactions

Xiaomei Lu [a,1], Jie He [a,1], Liang Huang [c,1], Jingzhong Qin [a], Yuandie Ma [a], Xianxiang Liu [b,*], Wenguang Zhao [b], Bing Liu [a], Zehui Zhang [a,*]

[a] Key Laboratory of Catalysis and Materials Sciences of the Ministry of Education, South-Central Minzu University, Wuhan 430074, PR China
[b] National & Local Joint Engineering Laboratory for New Petro-chemical Materials and Fine Utilization of Resources, Hunan Normal University, Changsha 410081, PR China
[c] The State Key Laboratory of Refractories and Metallurgy, Wuhan University of Science and Technology, Wuhan 430081, PR China

ARTICLE INFO

Keywords:
Catalytic transfer hydrogenation
Carbonyl group
Metal-free catalysts
Pyridinic nitrogen
Synergistic catalysis

ABSTRACT

Transition metal catalysts are commonly used for chemical reactions, especially for transfer hydrogenation reactions. From the viewpoints of green and sustainable chemistry, it is highly demanded to develop metal-free catalytic systems. Herein, oxygen-containing groups modified nitrogen-doped carbon catalysts were discovered to be robust for the transfer hydrogenation reaction between nitroarenes and saturated N-heterocyclic compounds, achieving high yields of anilines and unsaturated N-heterocyclic. Control experiments and characterization results indicate that pyridinic N and carbonyl groups are the active sites. Furthermore, DFT calculation indicate that pyridinic N serves the role in the capture of the H atom from the N−H site in N-heterocycles and carbonyl group assists to capture the H atom from the adjacent carbon site. The as-formed H• species are then transferred to nitro groups in nitroarenes to generate anilines. This amalgamation of multiple active sites reveals opportunities for developing modified metal-free carbon catalysts for extensive applications.

1. Introduction

Catalytic transfer hydrogenation (CTH), in which an acceptor molecule fetches hydrogen atoms from a donor molecule through an intermediate catalyst, has received enormous attention in recent years [1–3]. It is a simple, atom economic, and environmentally benign process that adopts a privileged position in various kinds of chemical reactions [4,5].

In general, the presence of transition metals is essential for transfer hydrogenation reactions due to their extraordinary hydrogen abstraction ability [6–8], namely transition metals can easily capture hydrogen atoms from the hydrogen donors to form an intermediate of metal hydride and then transfer the hydrogen atoms to the acceptor. Up to now, transition metal catalysts have been widely applied in some important transfer hydrogenation reactions, represented by the reduction of nitro compounds, quinoline, and furfural using iso-propanol or formic acid derivatives as the hydrogen donors [9–11]. Despite of the significant progress made in transition metal-catalyzed transfer hydrogenation reactions, transition-metal catalysts share common disadvantages such as high cost, limited availability, potential toxicity, and poor durability, owing to the inevitable leaching of metal species during the reaction [12,13]. Particularly, they are unfavorable in the drug and pharmaceutical industry, because the presence of trace metal residues must be isolated from the products through extra and strict separation processes. Therefore, developing metal-free catalysts for transfer hydrogenation reactions is highly desirable. However, the fabrication of efficient metal-free catalysts is still challenging, as it is hard to achieve dehydrogenation and hydrogenation simultaneously on a single metal-free surface [14].

Carbon materials, including amorphous carbon, ordered mesoporous carbon, graphite/graphene, and carbon nanotubes, are popular metal-free catalysts in various organic transformations [15–17]. To improve the catalytic performance of carbon catalysts, many modification strategies have been adopted, which typically introduce heteroatom (e.g., N, O, B, etc.) to create surface functionalities. After the doping, the charge density of carbon materials can be improved and the inert carbon materials are turned to be active for specific reactions [18,19]. In general, carbon materials are doped with a single kind of heteroatom (typically

* Correspondence authors.
E-mail addresses: lxx@hunnu.edu.cn (X. Liu), lxx@hunnu.edu.cn (Z. Zhang).
[1] These authors contributed equally to this work.

https://doi.org/10.1016/j.apcatb.2022.122277

Available online 9 December 2022

nitrogen), as the introduction of two or more heteroatoms usually results in the complexity of carbon structure as well as the difficulty in investigating active sites and catalytic mechanisms. Currently, nitrogen-doped carbon catalysts have been widely applied in thermal-catalytic and electrocatalytic reactions [20]. Besides the doping method, modifying carbon materials with surface oxygen-containing groups is another effective way [21,22]. For example, Kian et al. studied the synergistic effect of carboxylic acid groups and unpaired electrons in graphene oxide on the catalytic oxidative coupling of amines to imines. The carboxylic groups at the edges of defects, along with the localized unpaired electrons, work synergistically to trap molecular oxygen and the amine molecules, thus facilitating intermolecular arrangements [23]. Inspired by this, we speculate the combination of nitrogen doping and modifying with oxygen-containing groups might be feasible to improve the activity of carbon catalysts towards those valuable but challenging transfer hydrogenation reactions.

Anilines are a kind of important chemicals with wide applications in the synthesis of nitrogen-containing pharmaceuticals dyes, pesticides, and so forth [24,25]. The simple and effective way to access anilines is the reduction of nitroarenes by H_2 or other hydrogen donors. As far as the use of common hydrogen donors such as alcohols, formic acid, and borane ammonia for the transfer hydrogenation of nitroarenes [26–28], it still suffers some disadvantages in terms of the unsatisfactory atomic efficiency and the un-sustainability with use of additives. Thus, it would be interesting to use saturated organic molecules as the hydrogen donor for the transfer hydrogenation of nitroarenes into anilines with the simultaneous generation of other high-value chemicals. Similar to anilines, N-heterocyclic aromatic compounds, are also of great importance in a variety of applications [29]. Therefore, the integration of the dehydrogenation of saturated N-heterocycles into unsaturated N-heterocycles and the in-situ hydrogenation of nitroarenes into anilines in one pot would be more economic and sustainable to access nitrogen-containing compounds, but it has been rarely reported [30,31].

In this work, the oxygen-containing groups modified nitrogen-doped carbon is discovered to be active in the transfer hydrogenation reactions between nitroarenes and saturated N-heterocycles using H_2O as the green solvent. To the best of our knowledge, this is a previously unknown example on the use of heterogeneous metal-free materials to catalyze this transformation. The experimental results combined with DFT calculations suggest that pyridinic N and surface carbonyl groups are the active sites, working synergistically in the whole reaction process.

2. Experimental section

2.1. Materials

Dicyandiamide (99%), trimesic acid (98%), terephthalic acid (99%), pyromellitic acid (>98.0%) and D-(+)-glucose (99%) were purchased from Shanghai Aladdin Biochemical Technology Co., Ltd. (Shanghai, China). Organic solvents were purchased from Sinopharm Chemical Reagent Co., Ltd. (Shanghai, China). All reagents were used without further purification.

2.2. Preparation of oxygen-containing groups modified nitrogen-doped carbon

Oxygen-containing groups modified nitrogen-doped carbon (ONC) materials were prepared via a facile co-pyrolysis method. Typically, trimesic acid (0.2 g) and dicyandiamide (DCDA, 4.0 g) were mixed by grinding and annealed at 800 ℃ for 2 h in a tube furnace, with a heating rate of 5 °C min^{-1} under continuous N_2 flow. After naturally cooling down to room temperature, the as-prepared sample was obtained and grinded for the further use. During the optimization of preparation conditions, the amount of trimesic acid (g) and the annealing temperature (℃) were the variables. Therefore, the as-prepared samples were denoted as ONC_x-T (x represents the mass of trimesic acid and T is the pyrolysis temperature).

2.3. Preparation of ONC_{Te}-800 and ONC_{Py}-800

Terephthalic acid (with two carboxylic groups, 0.4 g) and pyromellitic acid (with four carboxylic groups, 0.4 g) were used to replace trimesic acid in the catalyst preparation. The preparation procedures remained the same and the obtained samples were donated as ONCTe-800 and ONCPy-800, respectively.

2.4. Preparation of C_3N_4

C_3N_4 was prepared according to the well-known method. Typically, DCDA (5 g) was placed in a crucible boat and heated at 550 °C under a continuous flow of N_2 for 4 h, with a heating rate of 2 °C min^{-1}.

2.5. Preparation of glucose-derived carbon (GMC-800)

Glucose (5 g) was added to a crucible boat and heated at 800 °C under a continuous flow of N_2 for 4 h, with a heating rate of 5 °C min^{-1}.

2.6. Preparation of N-doped carbon (NMC-800)

Glucose (5 g) and DCDA (5 g) were first mixed by grinding. The mixed powder was transferred into a crucible boat and heated to 800 °C under a continuous flow of N_2 for 4 h, with a heating rate of 5 °C min^{-1}.

2.7. Evaluation of catalytic performance for transfer hydrogenation reactions

Typically, 0.4 mmol of nitrobenzene, 0.6 mmol of 1,2,3,4-tetrahydroquinoline (THQ), 20 mg of $ONC_{0.4}$-800, and 10 mL of deionized water were added to a stainless-steel reactor. The reaction was filled with N_2 for 15 min to remove the air in the autoclave. The reactor was then sealed and heated from room temperature to 180 ℃ within several minutes. Then the reaction was started at 180 ℃ for a certain time with a stirring at 1000 rpm. After the reaction, the autoclave was cooled down with cold water. Ethylbenzene was added to the reaction mixture as an internal standard, and the products were analyzed through gas chromatograph-mass spectrometer and gas chromatography, respectively. In the recycling test, the catalyst was washed with deionized water and ethyl acetate, then dried for the next run with exact the same method.

2.8. Characterization

The morphology and particle size of the samples were observed and measured by transmission electron microscopy (TEM, JEM-2100 from JEOL). Powder X-ray diffraction (XRD) studies were conducted on a Rigaku RINT-2200 X-ray diffractometer with a Cu Kα source at 40 kV and 20 mA. X-ray photoelectron spectroscopy (XPS) measurements were performed on a Thermo Scientific ESCALAB 250Xi system equipped with a hemispherical analyzer and using a monochromatic Al Kα radiation source. The BET surface area, pore volume, pore size distribution, and average pore diameter of the samples were characterized by nitrogen adsorption/desorption analysis at 77 K on a Quantachrome Quadrasorb SI Instrument. Before the measurements, the samples were degassed at 150 ℃ for 4 h. Raman spectra were obtained in a LabRAM HR spectrometer with an excitation wavelength of 632 nm with 3 cm^{-1} spectral resolution. FT-IR spectra were obtained using the Nexus 470 instrument.

2.9. Theoretical method

The DFT calculations were carried out by VASP with the gradient-corrected PBE exchange-correction functional. The energy cutoff for

the plane waves was set to 400 eV. The Brillouin zone integration was performed using a Monkhorst-Pack grid of 2 × 2 × 1 special k-points. All the atomic positions were relaxed until all the remaining forces on these atoms are < 0.02 eV/Å. The transition states (TS) were searched by the "climbing images" nudged elastic band (CI-NEB) algorithm.

3. Results and discussion

3.1. Catalyst preparation and characterization

As illustrated in Fig. 1A, oxygen-containing groups modified nitrogen-doped carbon (ONC) were prepared via the direct co-pyrolysis of the composite of dicyandiamide (DCDA) and trimesic acid (TMA), which is simple and reproducible. The as-prepared carbon catalysts are abbreviated as ONC_x-T, where x and T represent the amount of trimesic acid and the pyrolysis temperature, respectively. $ONC_{0.4}$-800 is taken as the representative to study the microstructure of the as-prepared ONC catalysts. As evidenced by the transmission electron microscopy (Fig. 1B-E), $ONC_{0.4}$-800 possesses a few-layer sheet-like porous structure with numerous wrinkles and nanoholes randomly distributed in the plane. The interplanar distance of 0.35 nm was measured in the high-resolution TEM (HR-TEM) image of $ONC_{0.4}$-800 (Fig. 1E), assigning to the (002) face of graphitic carbon. This result is also confirmed by the X-ray diffraction spectra (Fig. S1). Only two broad diffusion peaks at 26.4° and 43.4° were observed in the $ONC_{0.4}$-700, $ONC_{0.4}$-800, and $ONC_{0.4}$-900 samples, which are ascribed to the (002) and (101) planes of graphitic carbon (PDF#41–1487). The $ONC_{0.4}$-700 and $ONC_{0.4}$-900 samples also show sheet-like structures (Fig. S2), suggesting that the pyrolysis temperature varying from 700 ℃ to 900 ℃ has little influence on the formation of sheet-like porous morphology.

The relative amount of the surface defects was studied by Raman spectroscopy, by comparing the intensity ratio of the D and G bands (I_D/I_G). The typical D band at around 1350 cm^{-1} represents the edges, defects, and disordered carbon sites, and the G band at 1580 cm^{-1} is attributed to the in-plane bond-stretching motion of pairs in sp^2-C atoms. A larger ratio of I_D/I_G generally indicates a higher content of disordered carbon and defect level [32]. As shown in Fig. 1F, the I_D/I_G values were calculated to be 1.07, 1.05, and 1.03 for $ONC_{0.4}$-700, $ONC_{0.4}$-800, and $ONC_{0.4}$-900, respectively, suggesting that the content of the defective carbon was lower at higher pyrolysis temperature. The carbon catalysts synthesized with different amounts of trimesic acid, namely $ONC_{0.2}$-800, $ONC_{0.4}$-800, and $ONC_{0.8}$-800 were also examined by Raman spectroscopy (Fig. S3). Among them, the $ONC_{0.4}$-800 sample possesses the largest I_D/I_G ratio. These results suggest that $ONC_{0.4}$-800 has the most abundant defective sites, despite the amount of trimesic acid used in its preparation was not the largest, which is probably due to the highest nitrogen content (11.9 at%), evidenced by the following XPS analysis.

Nitrogen adsorption-desorption isotherms and pore-size distribution of $ONC_{0.4}$-700, $ONC_{0.4}$-800, and $ONC_{0.4}$-900 are shown in Fig. 1G-H and Table S1. $ONC_{0.4}$-800 exhibits a specific surface area of 588 $m^2\ g^{-1}$, which is much higher than that of $ONC_{0.4}$-700 (383 $m^2\ g^{-1}$) and $ONC_{0.4}$-900 (448 $m^2\ g^{-1}$), and also higher than that of $ONC_{0.2}$-800 (379 $m^2\ g^{-1}$) and $ONC_{0.8}$-800 (44 $m^2\ g^{-1}$) (Fig. 1G and S4a). All samples dominantly possess micropores according to the pore-size distribution curves (Fig. 1H and Fig. S4b), while $ONC_{0.4}$-800 possess a wider pore-size distribution compared to the others. This observation is also confirmed by HR-TEM images (Fig. 1D). The $ONC_{0.4}$-800 catalyst with the largest surface area are attributed to its holey structure with abundant pores, which are expected to facilitate the exposure of active sites and benefits the mass transfer of the substrate/product molecules during the reaction process.

To gain further insights into the surface content and chemical status of elements on the ONC samples, XPS analysis were carried out (Fig. 2A-D). Firstly, the XPS spectra of the $ONC_{0.4}$-T samples were analyzed and compared. As can be seen in survey spectra (Fig. S5), the peaks with the binding energies located at ca. 284, 401, and 532 eV correspond to C 1 s, N 1 s, and O 1 s, respectively. The C 1 s spectra of all ONC samples were

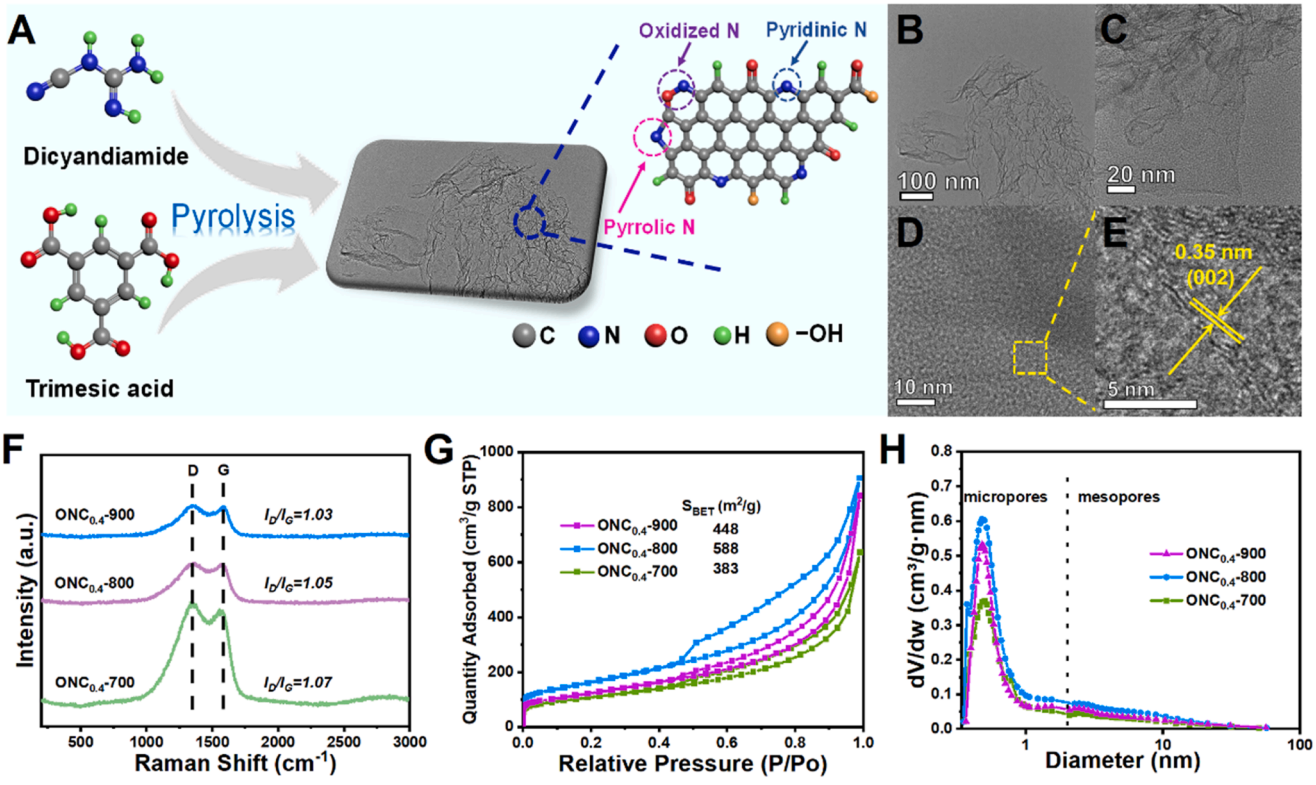

Fig. 1. Preparation and Characterization of the ONC Catalysts (A) Schematical illustration of the preparation of ONC_x-T catalysts; (B) TEM and (C-E) HR-TEM images of $ONC_{0.4}$-800; (F) Raman spectra, and (G-H) N_2 absorption-desorption curves and pore-size distribution of $ONC_{0.4}$-700, $ONC_{0.4}$-800, and $ONC_{0.4}$-900.

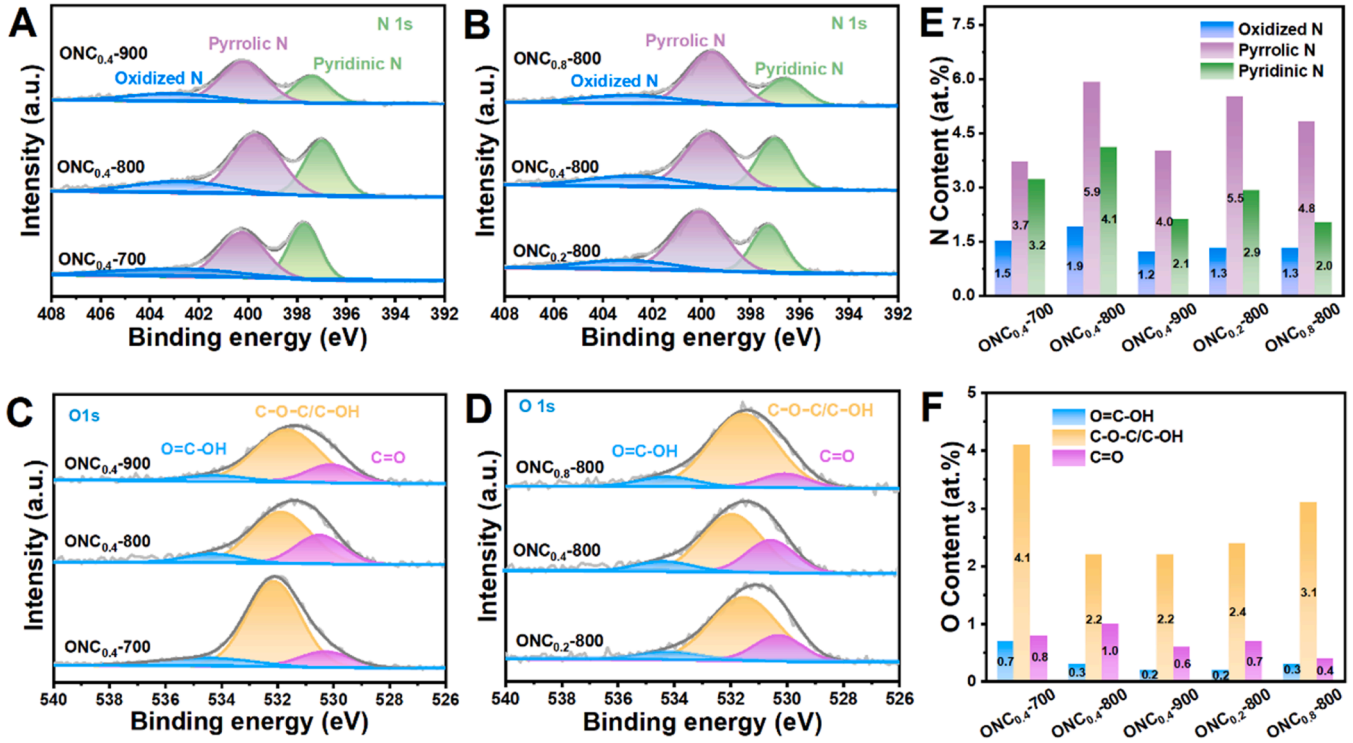

Fig. 2. Surface content and chemical status of elements on ONC catalysts (A) N 1 s and (C) O 1 s XPS spectra of $ONC_{0.4}$-700, $ONC_{0.4}$-800, and $ONC_{0.4}$-900; (B) N 1 s and (D) O 1 s XPS spectra of $ONC_{0.2}$-800, $ONC_{0.4}$-800, and $ONC_{0.8}$-800; quantitative analysis of N species (E) and O species (F) of different catalysts.

similar and could be divided into six different types (Fig. S6), including C−C/C−H/C═C (284.8 eV), C−O/sp^3 C/C═N (286.2 eV), C−N (287.5 eV), C═O (288.9 eV), O═C−OH (290.4 eV), and $\pi-\pi^*$ (292.2 eV) [33,34]. The N 1 s spectra were fitted to three different types [35,36], pyridinic N (397.6 eV), pyrrolic N (400.2 eV), and oxidized N (403.1 eV) (Fig. 2A and Table S2). The peak intensities for pyridinic N and pyrrolic N are much stronger than that of oxidized N, evidencing that N atoms were mainly doped into the carbon lattice. The O 1 s spectra can be divided into three types as follows [37], O═C−OH (534.3 eV), C−O−C/C−OH (531.9 eV), and C═O (530.5 eV) (Fig. 2C and Table S3). The existence of these O species was also confirmed by FT-IR spectra. As shown in Fig. S7, the peak at 3460 cm^{-1} represents the O−H stretching of the −COOH group, and the peaks at approximately 1670 and 1400 cm^{-1} represent carbonyl (C═O) and C−N band stretching groups, respectively [34,38]. Similar qualitative findings were recorded in the XPS spectra for $ONC_{0.2}$-800, $ONC_{0.4}$-800, and $ONC_{0.8}$-800 (Figs. 2B, 2D and S7).

A quantitative XPS analysis was conducted to determine the surface content of the N types and O types. Atomic percentages of pyridinic N, pyrrolic N, and oxidized N, as well as O═C−OH, C−O−C/C−OH, and C═O in different samples were calculated as follows: content of N_{Types}/O_{Types} (atomic %) = total content of N/O (atomic %) × the area of fitting percentage of N_{Types}/O_{Types} (%) by XPS (Fig. 2E-F, Tables S4-5 and S8–9) [39–41]. Higher pyrolysis temperature leads to a lower proportion of pyridinic N and pyrrolic N, but has less influence on oxidized N (Fig. 2E). For the samples prepared with different amounts of trimesic acid, the atomic proportions of pyrrolic N and oxidized N are close, but that of pyridinic N is quite different among these samples, $ONC_{0.4}$-800 possesses the highest content of pyridinic N (Table S4). Pyrolysis temperature showed negligible influence on the proportion of O═C−OH and C−O−C/C−OH except for $ONC_{0.8}$-800 (Table S5), which might be caused by the largest amount of trimesic acid used in its preparation. It was worth pointing out that among all the samples, $ONC_{0.4}$-800 possesses the highest proportion of both pyridinic N and carbonyl groups.

3.2. Catalytic performance of the as-prepared carbon catalysts

To investigate the catalytic performance of the as-prepared samples, the transfer hydrogenation reaction between nitrobenzene and 1,2,3,4-tetrahydroquinoline (THQ) was conducted as a model reaction. In this reaction, THQ serves as a hydrogen donor for the reduction of nitrobenzene into aniline, while water is generated as the sole by-product. The catalytic performances of different catalysts were initially screened in water at 180 ℃ (Table 1). As the benchmark reaction, no reaction occurred in the absence of carbon materials (Entry 1). To our great pleasure, the as-prepared carbon materials could promote the

Table 1
Catalytic performance of the transfer hydrogenation reaction between nitrobenzene and THQ [a].

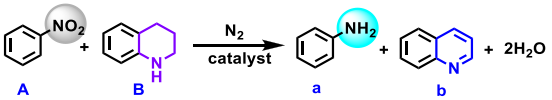

Entry	Catalyst	Conversion (%)		Yield (%)	
		A	B	a	b
1	-	–	–	–	–
	ONC0.4–700				
	ONC0.4–800				
	ONC0.4–900				
	ONC0.2–800				
	ONC0.8–800				
	ONC0.4–800				
2	$ONC_{0.4}$-700	33	31	32	31
3	$ONC_{0.4}$-800	36	40	36	40
4	$ONC_{0.4}$-900	31	32	31	32
5	$ONC_{0.2}$-800	29	31	27	30
6	$ONC_{0.8}$-800	8	11	8	9
7[b]	$ONC_{0.4}$-800	90	91	90	91

[a] Reaction conditions: nitrobenzene (0.4 mmol), THQ (0.6 mmol), catalyst (20 mg), H_2O (10 mL), N_2 (1 MPa), 180 °C, 4 h; [b] 24 h.

transfer hydrogenation reaction between nitroarenes and saturated N-heterocyclic compounds. It was noted that the pyrolysis temperature showed a slight influence on the activity of the $ONC_{0.4}$-T catalysts. $ONC_{0.4}$-800 catalyst displays slightly higher activity than $ONC_{0.4}$-700 and $ONC_{0.4}$-900, realizing the highest nitrobenzene conversion in 36% and.

THQ conversion in 40% with almost 100% selectivity of both aniline and quinoline products (Entries 3 vs 2 & 4). These results might be explained by the differences in the number of active sites and the specific surface areas among the samples, as evidenced by the nitrogen adsorption-desorption measurements (Fig. 1G). In contrast to the pyrolysis temperature, the amount of trimesic acid in the preparation of ONC_x-800 sample showed a great effect on the catalytic activity of them. The catalytic activity of $ONC_{0.2}$-800 was slightly lower than $ONC_{0.4}$-800, while $ONC_{0.4}$-800 showed much higher catalytic activity than $ONC_{0.8}$-800 (Entries 3 vs 5 & 6), which is closely associated with the differences in the types and contents of N dopants and surface oxygen-containing groups as discussed in detail in the following section. Controlling experiment of the dehydrogenation of THQ without nitrobenzene only gave a trace amount of quinoline (Table S6), which suggests that the reaction between nitrobenzene and THQ was the real transfer hydrogenation reaction.

Subsequently, we conducted the optimization of reaction conditions over the $ONC_{0.4}$-800 catalyst. First, the effect of solvent on this transformation was studied (Table S7). It was discovered that water was superior to any other common solvents for this catalytic system. To get an in-depth understanding of the solvent effect, we observed the phenomena of $ONC_{0.4}$-800 catalysts and substrates in solvents. The photos (Fig. S8) revealed the hydrophobic property of both substrates and $ONC_{0.4}$-800 catalyst, and the catalyst and substrate were dispersed evenly in ethanol and toluene solvents, so the $ONC_{0.4}$-800 catalysts and the hydrophobic substrates are more accessible to the active sites on the catalyst in water. Thus, based on the catalytic performance and the 12 principles of green chemistry [42], we introduce water as the optimized solvent. The use of water as the reaction solvent is preferable in chemistry, as it is cheap and sustainable to the environment [43–45]. More importantly, the use of water also facilitates the separation of the products by the simple decantation method. The effect of reaction temperature was then studied. The transfer hydrogenation reaction between nitrobenzene and THQ was sensitive to the reaction temperature (Fig. S9a). With the increase of the reaction temperature from 150 ℃ to 180 ℃, the yields of quinoline and aniline both increased. Under the reaction temperature of 180 ℃, the yields of quinoline and aniline over the reaction time are shown in Fig. S9b. Both products showed almost similar yield, which was increased evenly over the reaction time. Within the time range, no other products and the reaction intermediates were detected by GC-MS. Finally, by extending the reaction time to 24 h, 90% yield for aniline and 91% yield for quinoline were achieved (Table 1, Entry 7).

3.3. Substrate scope of the transfer hydrogenation reactions

With the achievement of the optimized reaction conditions, we further explored the scope of the developed method (Fig. 3~4). The transfer hydrogenation reaction between THQ and different kinds of nitroarenes was first investigated (Fig. 3). Notably, nitroarenes bearing with strong to weak electron-donating groups all showed excellent yields of the corresponding aniline derivatives (**3b~3n**). On the meanwhile, electron-withdrawing groups in nitroarenes also showed no significant influence on the catalytic efficiency, and the corresponding aniline derivatives were attained in high yields beyond 90%. Particularly, benzocaine (**3o**), a commonly used local anesthetic was successfully synthesized with a satisfactory yield (>99%). Besides the electronic properties of the substituted groups, the position of the substituted groups also showed no obvious influence on the activity of the substrates, delivering high yields of these corresponding products (**3b~3d**; **3l & 3m**; **3q~3s**; **3v &3w**). Furthermore, the $ONC_{0.4}$-800 catalyst was also effective for the substrates with two or three substituted groups as well as the fused-ring with much more large steric hindrance, giving rise to the corresponding products with high yields (**3 y~3a$_3$**).

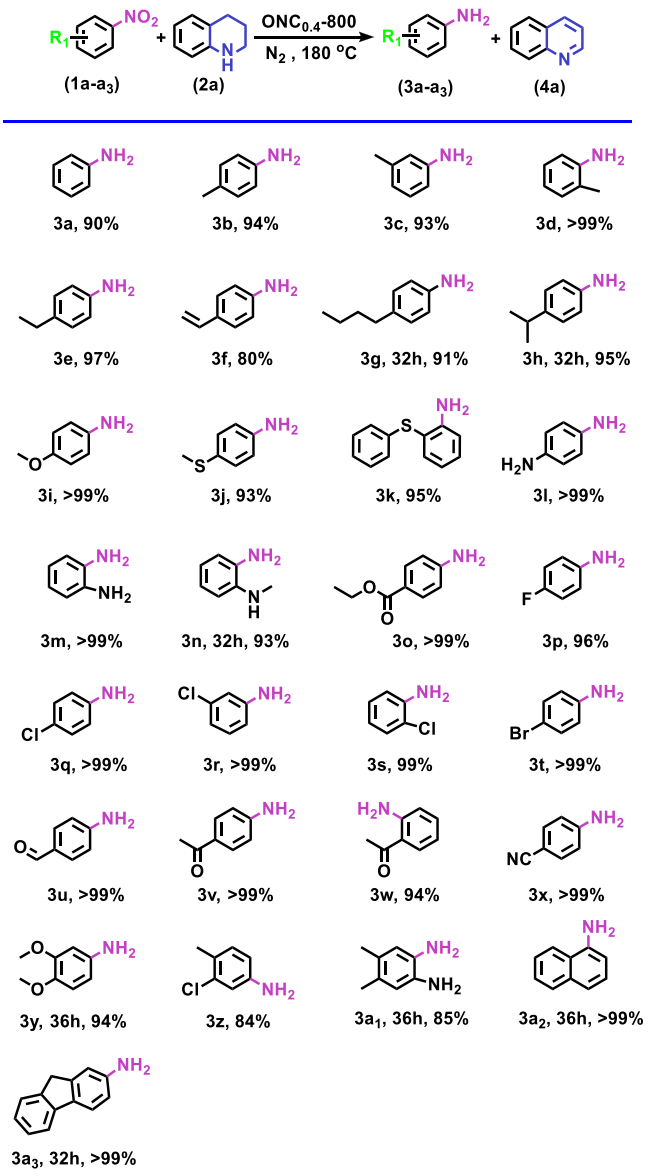

Fig. 3. Substrate scope of the transfer hydrogenation reactions between nitroarenes and 1,2,3,4-tetrahydroquinoline. Reaction conditions: nitroarenes (0.4 mmol), 1,2,3,4-tetrahydroquinoline (0.6 mmol), catalyst (20 mg), 180 ℃, H_2O (10 mL), N_2 (1 Mpa) and 24 h.

The catalytic system was also implemented to prepare aniline and unsaturated N-heterocycles from nitrobenzene and various kinds of saturated N-heterocycles. As shown in Fig. 4A, the $ONC_{0.4}$-800 catalyst was still workable under optimized conditions. Despite containing electron-donating or electron-withdrawing groups, the corresponding quinolines could be obtained with satisfactory yields. 6-methylquinoline (**8b**) and 6-methoxyquinoline (**8c**) were attained with yields of 96% and > 99%, respectively. By applying this method to synthesize isoquinoline derivatives, the products of isoquinoline (**8e**), 5-bromoisoquinoline (**8f**), and 6-hydroxy-isoquinoline (**8g**) were all obtained with yields higher than 98%. Substitutional groups had an obvious influence on the final products. When the substitutional group of phenyl was at the ortho-position of the nitrogen site, the yield of 1-phenylisoquinoline (**8i**) was 86% with a considerable amount of semi-dehydrogenation product

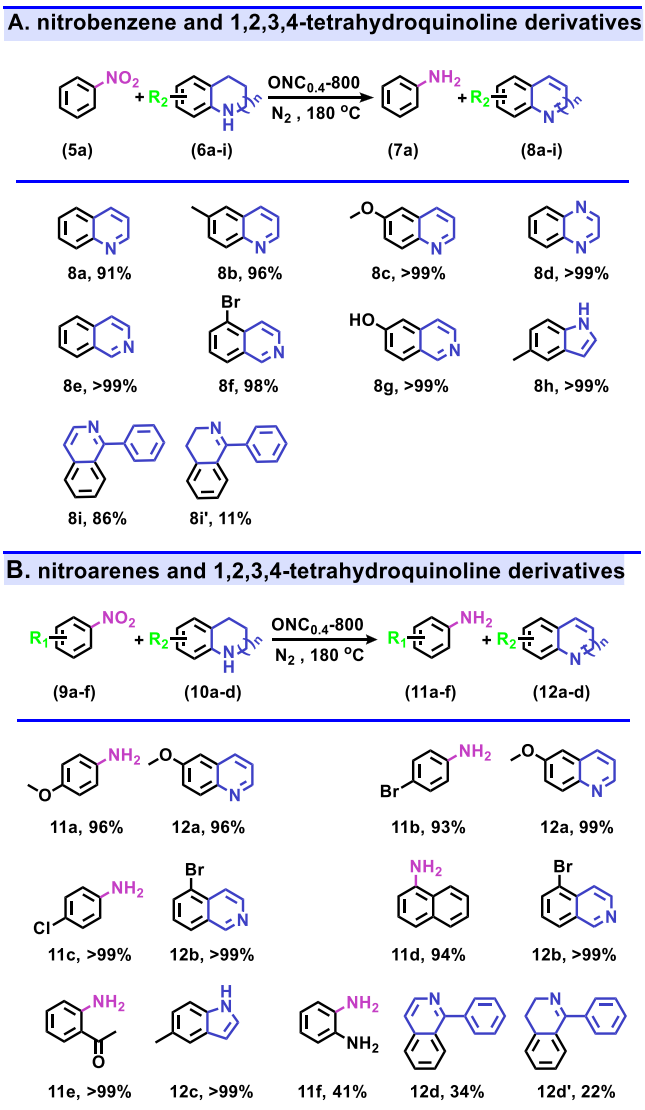

Fig. 4. Substrate scope of the transfer hydrogenation reactions between nitroarenes and saturated N-heterocyclic compounds. Reaction conditions: catalyst (20 mg), 180 °C, H_2O (10 mL), N_2 (1 Mpa) and 24 h. (A) nitrobenzene (0.4 mmol), 1,2,3,4-tetrahydroquinoline derivatives (0.6 mmol), (B) nitroarenes (0.4 mmol), 1,2,3,4-tetrahydroquinoline derivatives (0.6 mmol).

1-phenyl-3,4-dihydroisoquinoline (**8i'**). These results indicated that the dehydrogenation of N-heterocycles follows a step-by-step way, but the semi-dehydrogenation products of.

quinolines were not detected possibly due to the rapid dehydrogenation of THQ. In addition, some other nitrogen-containing heterocycles including quinoxaline (**8d**) and 5-methylindole (**8h**) were also successfully synthesized with quantitative yields.

The reaction also proceeded successfully with other structurally and electronically diverse nitrobenzene compounds and N-heterocycles (Fig. 4B). Corresponding aniline compounds (**11a-e**), quinoline compounds (**12a** or **12b**), and indole compound (**12c**) could be synthesized with excellent yields. Still, large steric hindrances in the substrate molecule also resulted in low product yields (**12d** and **12d'**). As listed in Fig. 3~4, the $ONC_{0.4}$-800 catalyst demonstrated a very broad range of substrate scope with good tolerance to many kinds of functional groups such as halogen, carbonyl, vinyl, and nitrile groups, demonstrating a promising application, while these functional groups are easily subjected to be reduced over metal catalysts. For example, the selective reduction of the nitro group in 4-nitrostyrene rather than vinyl group (C═C bond) to obtain 4-vinylaniline is a vital process in the production of antitumor agent Erlotinib and intermediates of fluorescent labels [46,47]. Generally, conversational catalysts usually resulted in the simultaneous hydrogenation of the vinyl group and nitro group, Au/SiO_2 catalysts are a good example, since they are able to hydrogenate successfully chlorinated nitrobenzenes, nitrotoluenes, nitrophenols and alkoxy nitrobenzenes [48], but they are non-selective for the hydrogenation of 3-nitrostyrene [49], leading to a poor selectivity of 3-vinylaniline, as the hydrogenation of vinyl group is more favourable than $-NO_2$ group both kinetically and thermodynamically. To realize the selective reduction of 4-nitrostyrene into 4-vinylaniline, different kinds of noble metal-based catalysts with the assistance of second metal to form alloy nanoparticles such as CoRu, RuNi, and IrMo [50–52], or metal oxides such as Pt-FeO_x and Pd-CeO_2 were fabricated to selectively adsorb nitro group instead of vinyl group [53,54]. The good tolerance to the vinyl group in our catalytic system should be due to the introduction of oxygen-containing groups as well as the N atoms in the carbon materials, which created the surface of carbon materials to be polar and thus inhibit the adsorption of the vinyl group.

Besides the wide substrate scope, we are also interested in the practical application of our developed method. First, the gram-scale reactions were performed to evaluate the efficiency of this catalytic system (Fig. 5A). 92% of aniline and 93% of quinoline were still obtained by the reaction between nitrobenzene and THQ, which is comparable to the small-scale result. The gram-scale reaction was also successful over the reaction between 1,2-dimethoxynitrobenzene and 1,2,3,4-tetrahydroisoquinoline. Furthermore, the gram-scale reactions under solvent-free conditions were also conducted, and they were also successful with excellent yields (Fig. 5B). Moreover, the $ONC_{0.4}$-800 catalyst could be reused for 6 cycles without any obvious decline in catalytic efficiency (Fig. S10). Characterizations of cycle $ONC_{0.4}$-800 catalyst exhibited that the number of catalyst active sites as well as the structure did not change significantly by XRD, Raman spectroscopy and XPS (Fig. S11 and Tables S8-9), which further indicate that the loss of active centers is not likely to occur rapidly during the reaction and the catalyst has good stability. All these experimental results show that the $ONC_{0.4}$-800 has the industrial potential in large-scale synthesis. Overall, the ONC catalytic system offers a synthetically powerful method for metal-free catalytic transfer hydrogenation between nitroarenes and N-heterocycles.

3.4. Identification of active sites

To better understand the origin of the excellent catalytic activity of

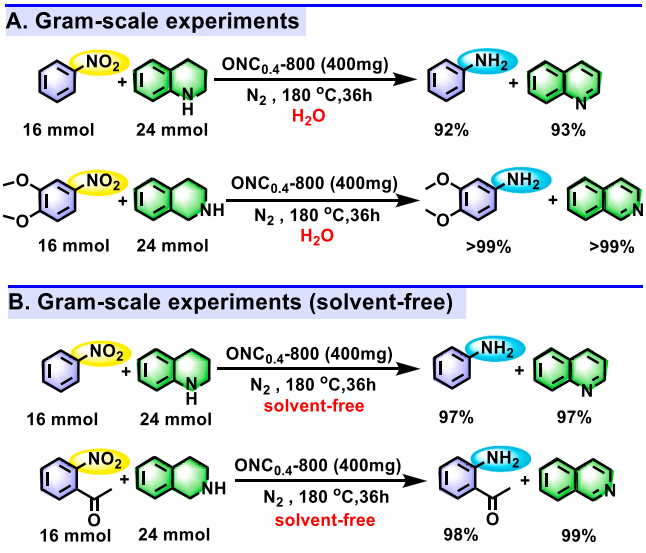

Fig. 5. (A) Gram scale experiments; (B) Gram scale experiments (solvent-free).

carbon materials, the catalytic active sites of the ONC catalysts are needed to be identified as a priority. It has been demonstrated in the literature that the introduction of nitrogen can provide carbon catalysts with active sites for dehydrogenation reactions [55], and the introduction of the C═O groups in carbon catalysts provides active sites for reductive hydrogen atom transfer reactions [14]. Thus, we speculate that both the nitrogen doping and surface modification with oxygen-containing groups had positive effects on catalytic performances. Three types of nitrogen including pyridinic N, pyrrolic N, and oxidized N, and three types of oxygen-containing groups including O═C−OH, C−O−C/C−OH, and C═O have been detected on the catalyst surface by XPS technology (Fig. 2A-D). Subsequently, a quantitative analysis based on the results of XPS and catalytic efficiencies was carried out to check out which nitrogen types and oxygen species are closely linked to the catalytic performance. As shown in Fig. 6, $ONC_{0.4}$-800 had superior activity to $ONC_{0.4}$-700 and $ONC_{0.4}$-900, while it also possesses the highest carbonyl and pyridinic N content and specific surface area (Fig. S12, Table S1). When comparing $ONC_{0.4}$-800 with $ONC_{0.2}$-800 and $ONC_{0.8}$-800, richer content of both pyridinic N and carbonyl groups was observed. Therefore, we deduce that both pyridinic N and carbonyl groups are plausible active sites, and a larger surface area is beneficial for gaining activity.

To verify the above statement, we carried out some controlling experiments to get more evidence (Table S10). C_3N_4 prepared by the calcination of DCDA under nitrogen atmosphere generally possesses pyridinic N, but no oxygen species on the catalyst surface. The characteristic peaks of FT-IR spectra for C_3N_4 were observed at 809 and 1200–1700 cm^{-1}, which belong to the deformation of tri-s-triazine ring modes and typical C–N heterocyclic stretches, respectively, and the broad peaks between 3000 and 3500 cm^{-1} were attributed to the combined symmetric and antisymmetric stretch vibrations of $-NH_2$ and −OH groups (Fig. S13) [56,57]. C_3N_4 showed no activity in the transfer hydrogenation reaction, suggesting that pyridinic N alone could not catalyze the reaction. Moreover, we inspected another carbon catalyst, namely GMC-800, prepared by the pyrolysis of glucose under an N_2 atmosphere at 800 ℃. Since glucose has rich oxygen-containing groups (including carbonyl groups), the resulted sample also contained oxygen species on the surface (Fig. S14). GMC-800 displayed a 7% yield of both products, much lower than that of $ONC_{0.4}$-800 (36% & 40%) under the same conditions. It proved that the existence of oxygen-containing groups alone on the carbon catalyst could catalyze the reaction in principle, but not as efficient as that of $ONC_{0.4}$-800. Furthermore, we came up to test a catalyst prepared using oxygen-rich glucose and nitrogen-rich DCDA as precursors via simple pyrolysis. However, this catalyst (NMC-800) showed a similar performance to GMC-800 and the XPS spectrum (Fig. S15) indicates that NMC-800 did not contain obvious carbonyl groups on its surface. This finding reminds us that the presence of the carboxylic acids in the presence of precursor was essential to forming the catalyst with synergetic pyridinic N sites and carbonyl groups.

In addition, we have supplemented XRD, Raman, and N_2 adsorption/desorption measurements for the C_3N_4, GMC-800, and NMC-800 samples, respectively, as shown in Fig. S16. The XRD pattern (Fig. S16a) of C_3N_4 displays two typical characteristic peaks including a small one at 13.2° corresponding to the tri-s-thiazine units (100), and a strong peak at 27.5° representing the inter-layer stacking of conjugated aromatic systems, which is indexed for graphitic materials as the (002) peak [58]. GMC-800 and NMC-800 have two weak and broad peaks at around 25° and 44°, which are assigned to the (002) and (101) planes of graphite carbon [59]. These results demonstrate that the C_3N_4, GMC-800, and NMC-800 samples has similar crystal plane with $ONC_{0.4}$-800. Raman spectra of NMC-800 and GMC-800 show two peaks with Raman shift at 1342 and 1582 cm^{-1} (Fig. S16b), which are associated with the disordered carbon (called the D band) and the crystalline graphitic carbon (called the G band), respectively. The I_D/I_G values of NMC-800 and GMC-800 are 0.97 and 1.00 respectively, which are lower than $ONC_{0.4}$-800 (1.05) catalyst and suggest that $ONC_{0.4}$-800 has the most abundant defective sites. N_2 absorption-desorption curves and pore-size distribution of C_3N_4, GMC-800, and NMC-800 are show in Fig. S16c-d and Table S11, the specific surface area of C_3N_4 (40 m^2 g^{-1}), GMC-800 (1 m^2 g^{-1}), and NMC-800 (31 m^2 g^{-1}) are lower than $ONC_{0.4}$-800 (588 m^2 g^{-1}), also, the $ONC_{0.4}$-800 possess a widest pore-size distribution compared to the C_3N_4, GMC-800, and NMC-800.

Based on this conclusion, we tried to use terephthalic acid with two carboxylic groups and pyromellitic acid with four carboxylic groups as precursors to prepare corresponding catalysts, namely ONC_{Te}-800 and ONC_{Py}-800, trying to distinguish the effect of precursors containing different amounts of carboxylic groups on catalytic activity. ONC_{Te}-800 and ONC_{Py}-800 catalysts had similar activities (Table S10), which were higher than C_3N_4, GMC-800, and NMC-800, but still lower than $ONC_{0.4}$-800, which was prepared using the precursor with three carboxylic groups. The optimization of carboxylic acid precursors suggested that trimesic acid was the most suitable one to result in the best catalyst. We prepared ONC_{TE}-800 and ONC_{PY}-800 to prove that the precursor containing different amounts of carboxylic acid groups has an effect on the active sites in the catalyst. In order to further confirm that carbonyl and pyridine nitrogen are the active sites for the synergistic catalytic hydrogenation reactions, we carried out XPS characterization on ONC_{TE}-800 and ONC_{PY}-800 and provided the relationship file between the types and contents of N and O species on different catalysts and catalytic activity (Fig. S17), it is found that their catalytic activities are positively associated with the content of pyridine nitrogen and carbonyl: for the three samples, the content of pyridine nitrogen and carbonyl follows the order of $ONC_{0.4}$-800 > ONC_{PY}-800 > ONC_{TE}-800 (Table S12 and S13), this trend is exactly consistent with the variation tendency of the yield of aniline and quinoline, $ONC_{0.4}$-800 (36%, 40%) > ONC_{PY}-800 (22%, 30%)> ONC_{TE}-800 (26%, 27%) (Table S10). Based on the above discussion, we conclude that the pyridinic N and carbonyl groups are both

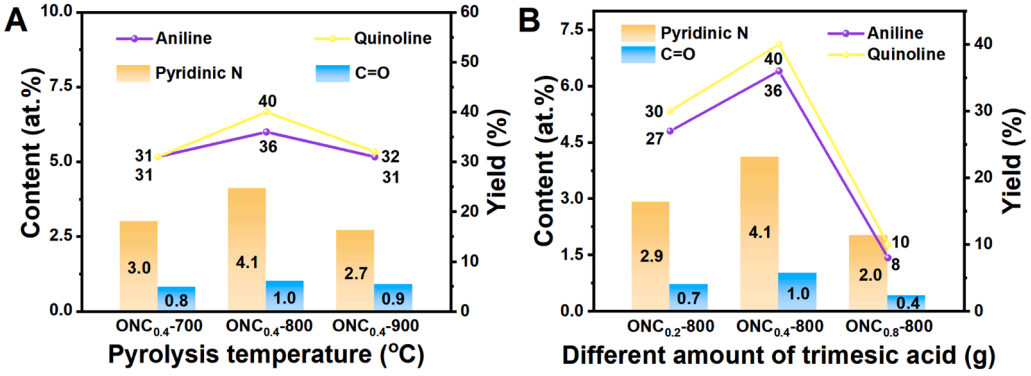

Fig. 6. Identification of active sites (A-B) The relationship between the types and contents of N and O species and catalytic activity.

the catalytic active sites, which synergistically promote the transfer hydrogenation reaction.

3.5. Mechanistic studies

In the transition-metal catalytic systems, nitrosobenzene and 1,2-dihydroquinoline are recognized intermediates in the catalytic transfer hydrogenation reaction between nitrobenzene and THQ. Since both the dehydrogenation and hydrogenation mechanisms with metal-free carbon catalysts are quite different from that of the transition-metal catalytic systems, we tried to explore the detailed mechanisms with both control experiments and DFT calculations.

Control experiments were first performed (Fig. 7). The electrical state of the active hydrogen species (H*) can be polar (hydride and proton, $H^{\delta-}$ and $H^{\delta+}$) and nonpolar (radical, $H^{\delta0}$). If H* exists in an electronic neutral state, hydrogen radicals must be involved in the reaction [30]. We attempted to add butylated hydroxytoluene (BHT, 2 equiv) to the reaction mixtures before the reaction started and a considerable decrease in catalytic activity was observed. As BHT is commonly used as the radical scavenger, this result suggests that catalytic transfer hydrogenation between nitrobenzene and THQ over the $ONC_{0.4}$-800 catalyst involves free radical intermediates (Fig. 7A). To further distinguish the pathway of the transfer hydrogenation processes, the reaction between nitrobenzene and 1,2,3,4-tetrahydroisoquinoline was performed over the $ONC_{0.4}$-800 catalyst at 180 °C for 4 h and the 3,4-dihydroisoquinoline intermediate was detected by GC-MS (Fig. 7C). But the use of 2-ethyl-1,2,3,4-tetrahydroisoquinoline without an N−H bond gave no dehydrogenation product (Fig. 7B). These results demonstrate that the formation of C=C bond is not preferential, and the existence of N−H bond is essential for the dehydrogenation of N-heterocycles. In the relevant studies on the dehydrogenation of THQ, the isomerization of 3,4-dihydroquinoline to 1,2-dihydroquinoline was an indispensable step to generate the dehydrogenation product of quinoline from THQ [55,60,61]. Thus, we deduced that the isomerization step was still involved in our metal-free catalytic routes.

On the basis of experimental results, we further carried out DFT calculations to explore the reaction mechanism. The model of the oxygen-containing modified nitrogen-doped carbon catalyst is illustrated in Fig. S18. The energy profile of the dehydrogenation of THQ is shown in Fig. 8A. Firstly, a THQ molecule adsorbs on the surface of ONC material with an adsorption energy of − 0.31 eV. The N−H bond of THQ (IS1) is then cleaved to generate the active H• species, and the H• tends to be transferred to the pyridinic N site via transition state TS1 with the energy barrier of 0.57 eV, as the energy barrier (> 1.00 eV) of the transfer the H• from N−H to the carbonyl site is much higher (Fig. S9b). Then the new N−H• bond is formed with a bond distance of 2.109 Å (IS2) (Fig. S20). Since this process has the highest energy barrier in the dehydrogenation process, it is the rate-determining step. Subsequently, another H• (originally bonded with the carbon adjacent to the N atom in the THQ molecule) is transferred to the oxygen atom in the carbonyl group on the catalyst surface via transition state TS2 with the energy barrier of 0.49 eV, to give rise to the 3,4-dihydroquinoline (IS3). Then, isomerization of 3,4-dihydroquinoline affords 1,2-dihydroquinoline (IS4). A similar dehydrogenation process subsequently proceeds with 1,2-dihydroquinoline as the benchmark. The H bonded with the N atom is transferred to a clean pyridinic N site via TS3 with the energy barrier of 0.53 eV and IS5 is produced. Then the final H bonded to the C atom is transferred to the oxygen atom in the carbonyl group via TS4 with the energy barrier of 0.07 eV to generate the final dehydrogenation product of quinoline (IS6).

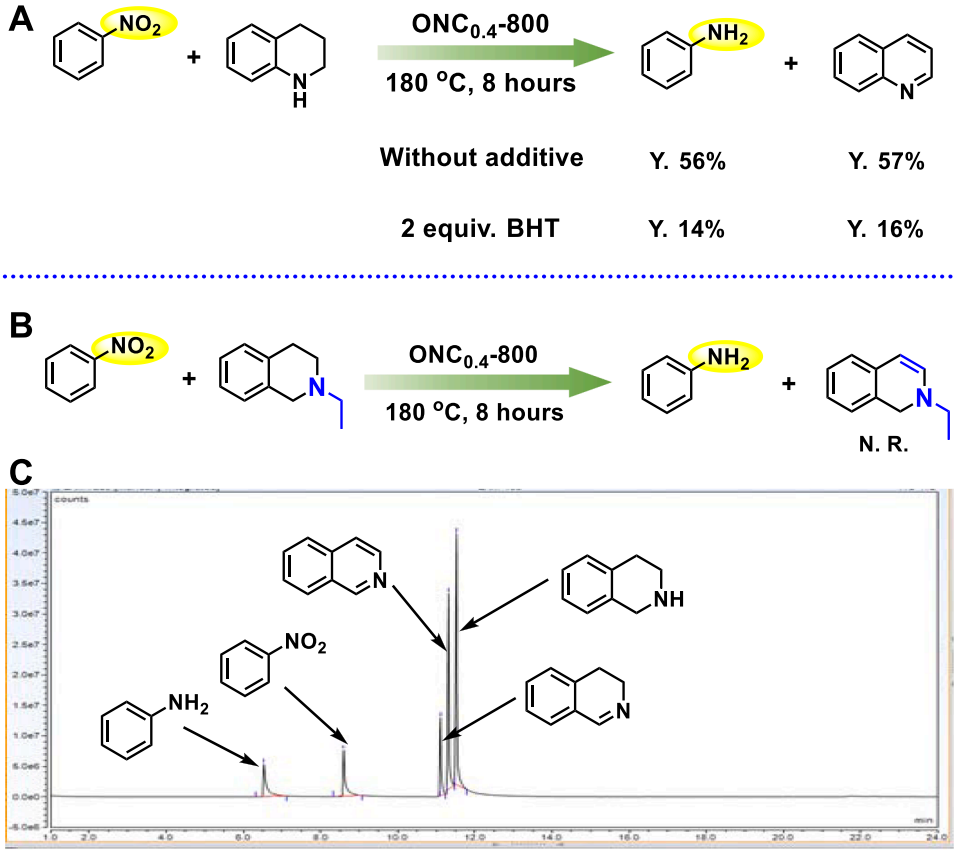

Fig. 7. Control experiments (A) Reaction condition: $ONC_{0.4}$-800 (20 mg), H_2O (10 mL), N_2 (1 MPa), 180 °C, 8 h. nitrobenzene (0.4 mmol), THQ (0.6 mmol); (B) nitrobenzene (0.4 mmol), 2-ethyl-1,2,3,4-tetrahydroisoquinoline (0.6 mmol), and otherwise conditions were the same for (A); (C) nitrobenzene (0.4 mmol), 1,2,3,4-tetrahydroisoquinoline (0.6 mmol), 4 h, and otherwise conditions were the same for (A).

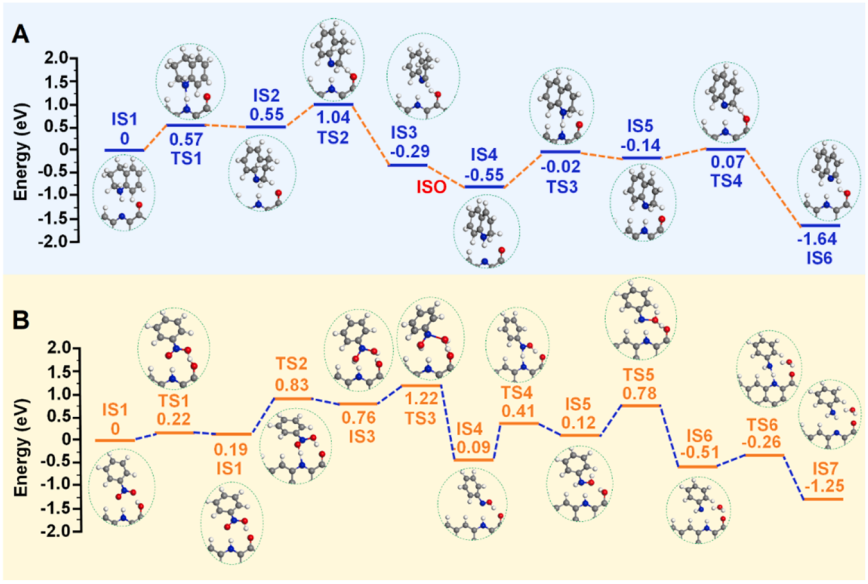

Fig. 8. Theoretical insights into the transfer hydrogenation reaction between nitrobenzene and 1,2,3,4-tetrahydroquinoline (A) The energy profile of the dehydrogenation of THQ; (B) The energy profile of the hydrogenation of nitrobenzene.

The energy profile of the hydrogenation of nitrobenzene shown in Fig. 8B. The H• abstracted by the carbonyl group is transferred to the oxygen atom of nitrobenzene to form an O−H bond (IS2) via TS1 with the energy barrier of 0.22 eV. It is not likely that the H• abstracted by pyridine N would be transferred to this oxygen atom in priority, as its energy barrier is much higher (> 0.75 eV, Fig. S21b). Then, the H• abstracted by pyridinic N is transferred to the other oxygen atom of nitrobenzene to form another O−H bond via TS2 (0.64 eV) to obtain the

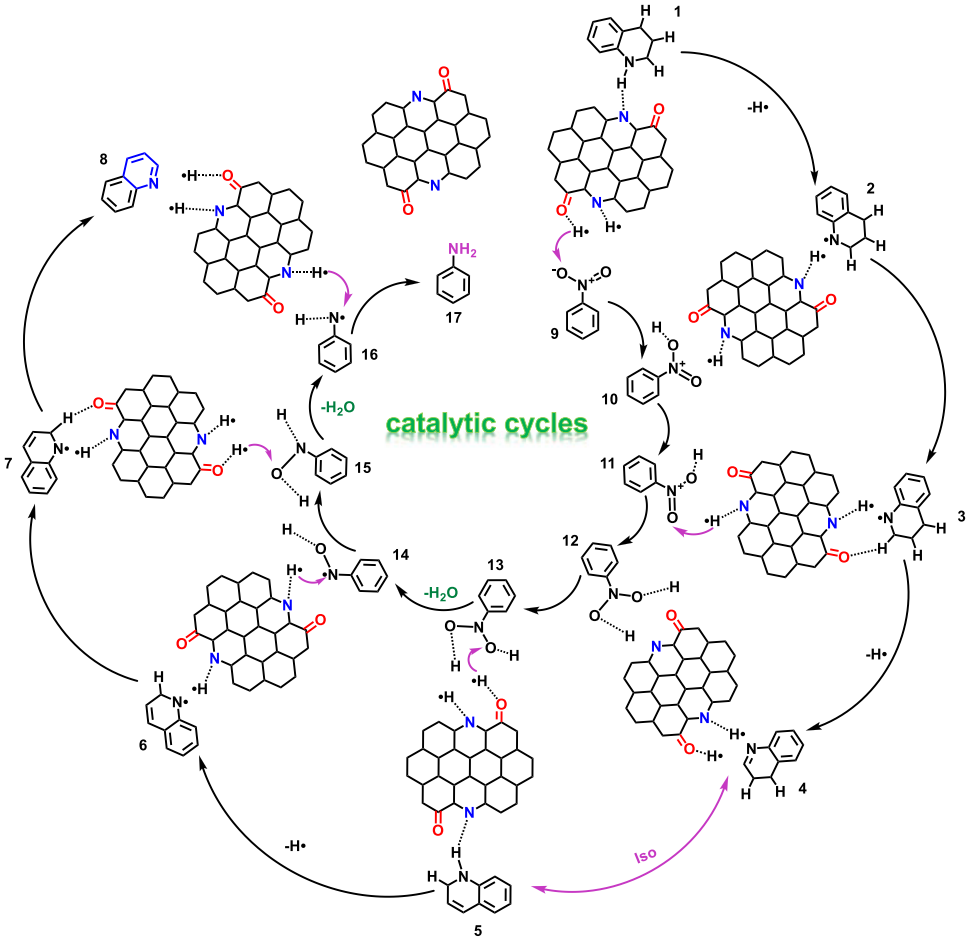

Fig. 9. The proposed reaction mechanism.

N, N-dihydroxyaniline intermediate (IS3). However, the self-condensation of IS3 to release water molecule with the energy barrier of 2.05 eV (Fig. S22a) or the isomerization of IS3 with the energy barrier of 1.99 eV (Fig. S22b) are both very difficult. Thus, IS3 prefers to interact with another H• abstracted by the carbonyl group to dehydrate one H_2O molecule to form IS4 via TS3, which has a much low energy barrier of 0.46 eV. Noting that this process is not preferred to undergo with H• abstracted by pyridinic N with a high energy barrier (> 0.46 eV, Fig. S23b). Next, another H• abstracted by pyridinic N is then added to the N atom in IS4 to form IS5 via TS4 with the energy barrier of 0.50 eV. Similarly, the other O−H in IS5 interacts with another H• abstracted by the carbonyl group to form IS6 via TS5 with the energy barrier of 0.66 eV, this step occupies the highest energy in the whole process and should be the rate-determining step. Finally, another H• abstracted pyridinic N is added to the N atom in IS6 via TS6 with the energy barrier of 0.25 eV, and the product aniline (IS7) is obtained.

As seen from the above analysis, the plausible mechanism of transfer hydrogenation reaction between nitroarenes and saturated N-heterocyclic compounds is proposed (Fig. 9). The H atoms of the saturated N-heterocyclic compounds are abstracted by the synergetic pyridinic N and carbonyl sites to generate the active H• species, then the active H• species are transferred through multiple steps to reduce nitroarenes, with H_2O as the only by-product during the whole process. Our mechanistic studies provide a rational understanding of this catalytic transformation from a molecular level.

4. Conclusions

In conclusion, we present oxygen-containing groups modified nitrogen-doped carbon catalysts with excellent catalytic performance for the transfer hydrogenation reactions between nitroarenes and saturated N-heterocycles. The quantitative analysis combined with control experiments suggests that pyridinic N and carbonyl groups are the active sites. Based on the control experiments and theoretical studies, we propose a plausible mechanism that pyridinic N and carbonyl group work synergistically in the capture and transfer of H atoms, which is markedly different from that with transitional metal catalytic systems. The developed method demonstrated some distinct advantages mainly including the facile preparation of metal-free carbon catalyst with low cost, the clean reaction without any additive and by the use of water as the solvent, the high catalytic efficiency with a good tolerance to some easily reductive groups, and the good potential in the industrial application with the high efficiency in gram-scale reactions under solvent-free conditions.

CRediT authorship contribution statement

Xiaomei Lu: Conceptualization, Investigation, Data curation, Formal analysis. **Jie He:** Conceptualization, Formal analysis, Writing–original draft, Project administration, Funding acquisition. **Liang Huang:** DFT calculation. **Jingzhong Qin:** Conceptualization, Data curation, Formal analysis, Investigation. **Yuandie Ma:** Formal analysis. **Xianxiang Liu**: Writing – review & editing, Funding acquisition. **Wenguang Zhao**: Formal analysis**. Bing Liu:** Formal analysis. **Zehui Zhang:** Supervision, Project administration, Writing – review & editing, Funding acquisition.

Declaration of Competing Interest

The authors declare that they have no known competing financial interests or personal relationships that could have appeared to influence the work reported in this paper.

Data availability

Data will be made available on request.

Acknowledgments

The authors thank the National Natural Science Foundation of China (22209210, 22278121, 21922513 and 21872175), the Natural Science Foundation of Hubei Province (No.2020CFA096), Fundamental Research Funds for Central Universities (CSZY22011, CZQ21008, and CZP20001), Scientific Research Fund of South-Central Minzu University (YZZ21005), and the Knowledge Innovation Program of Wuhan-Shuguang Project (2022010801020411).

Appendix A. Supporting information

Supplementary data associated with this article can be found in the online version at doi:10.1016/j.apcatb.2022.122277.

References

[1] Z.-J. Gong, Y.S.L.V. Narayana, Y.-C. Lin, W.-H. Huang, W.-N. Su, Y.-P. Li, M. Higuchi, W.-Y. Yu, Rational synthesis of ruthenium-based metallo-supramolecular polymers as heterogeneous catalysts for catalytic transfer hydrogenation of carbonyl compounds, Appl. Catal. B: Environ. 312 (2022), 121383.
[2] Y.Y. Ren, Y.S. Yang, L.F. Chen, L. Wang, Y.W. Shi, P. Yin, W.L. Wang, M.F. Shao, X. Zhang, M. Wei, Synergetic effect of Cu^0 −Cu^+ derived from layered double hydroxides toward catalytic transfer hydrogenation reaction, Appl. Catal. B: Environ. 314 (2022), 121515.
[3] M.J. Gilkey, B.J. Xu, Heterogeneous catalytic transfer hydrogenation as an effective pathway in biomass upgrading, ACS Catal. 6 (2016) 1420–1436.
[4] J.R.D. Iorio, B.A. Johnson, Y. Roman-Leshkov, Ordered hydrogen-bonded alcohol networks confined in lewis acid zeolitesaccelerate transfer hydrogenation turnover rates, J. Am. Chem. Soc. 142 (2020) 19379–19392.
[5] M.F. Pang, J.-Y. Chen, S.J. Zhang, R.-Z. Liao, C.-H. Tun, W.G. Wang, Controlled partial transfer hydrogenation of quinolines by cobalt-amido cooperative catalysis, Nat. Commun. 11 (2020) 1249.
[6] R.F. Nie, Y.W. Tao, Y.Q. Nie, T. Lu, J.S. Wang, Y.S. Zhang, X.Y. Lu, C.B.C. Xu, Recent advances in catalytic transfer hydrogenation with formic acid over heterogeneous transition metal catalysts, ACS Catal. 11 (2021) 1071–1095.
[7] J.S.M. Samec, J.-E. Backvall, P.G. Andersson, P. Brandt, Mechanistic aspects of transition metal-catalyzed hydrogen transfer reactions, Chem. Soc. Rev. 35 (2006) 237–248.
[8] K.K. Sun, H.B. Shan, G.-P. Lu, C. Cai, M. Beller, Synthesis of N-heterocycles via oxidant-free dehydrocyclization of alcohols using heterogeneous catalysts, Angew. Chem. Int. Ed. 60 (2021) 2–17.
[9] P. Zhou, Z.H. Zhang, L. Jiang, C.L. Yu, K. Lv, J. Sun, S.G. Wang, A versatile cobalt catalyst for the reductive amination of carbonyl compounds with nitro compounds by transfer hydrogenation, Appl. Catal. B: Environ. 210 (2017) 522–532.
[10] Y.H. Han, Z.Y. Wang, R.R. Xu, W. Zhang, W.X. Chen, L.R. Zheng, J. Zhang, J. Luo, K.L. Wu, Y.Q. Zhu, C. Chen, Q. Peng, Q. Liu, P. Hu, D.S. Wang, Y.D. Li, Ordered porous nitrogen-doped carbon matrix with atomically dispersed cobalt sites as an efficient catalyst for dehydrogenation and transfer hydrogenation of N-heterocycles, Angew. Chem. Int. Ed. 57 (2018) 11262–11266.
[11] G.-H. Wang, X.H. Deng, D. Gu, K. Chen, H. Tîysîz, B. Spliethoff, H. Bongard, C. Weidenthaler, W. Schmidt, F. Schîth, Co_3O_4 nanoparticles supported on mesoporous carbon for selective transfer hydrogenation of a,β-unsaturated aldehydes, Angew. Chem. Int. Ed. 55 (2016) 11101–11105.
[12] K.Z. Wang, P.B. Jiang, M. Yang, P. Ma, J.H. Qin, X.K. Huang, L. Ma, R. Li, Metal-free nitrogen-doped carbon nanosheets: a catalyst for the direct synthesis of imines under mild conditions, Green. Chem. 21 (2019) 2448–2461.
[13] A.D. Sutton, A.K. Burrell, D.A. Dixon, E.B. Garner, J.C. Gordon, T. Nakagawa, K. C. Ott, J.P. Robinson, M. Vasiliu, Regeneration of ammonia borane spent fuel by direct reaction with hydrazine and liquid ammonia, Science 331 (2011) 1426–1429.
[14] H.M. Yang, X.J. Cui, X.C. Dai, Y.Q. Deng, F. Shi, Carbon-catalysed reductive hydrogen atom transfer reactions, Nat. Commun. 6 (2015) 6478.
[15] X.-K. Kong, C.-L. Chen, Q.-W. Chen, Doped graphene for metal-free catalysis, Chem. Soc. Rev. 43 (2014) 2841–2857.
[16] K. Chen, Y.B. Li, M.H. Wang, Y.H. Wang, K. Cheng, Q.H. Zhang, J.C. Kang, Y. Wang, Functionalized carbon materials in syngas conversion, Small 17 (2021) 2007527.
[17] Y. Fang, Y.X. Liu, L. Qi, Y.R. Xue, Y.L. Li, 2D graphdiyne: an emerging carbon material, Chem. Soc. Rev. 51 (2022) 2681–2709.
[18] H.T. Hu, Y.Q. Nie, Y.W. Tao, W.Y. Huang, L. Qi, R.F. Nie, Metal-free carbo catalyst for room temperature acceptorless dehydrogenation of N-heterocycles, Sci. Adv. 8 (2022) 9478.
[19] J.W.F. To, J.J. He, J.G. Mei, R. Haghpanah, Z. Chen, T. Kurosawa, S.C. Chen, W.-G. Bae, L.J. Pan, J.B.-H. Tok, J. Wilcox, Z.A. Bao, Hierarchical N-doped carbon as CO_2 adsorbent with high CO_2 selectivity from rationally designed polypyrrole precursor, J. Am. Chem. Soc. 138 (2016) 1001–1009.
[20] J. Oh, S. Park, D. Jang, Y. Shin, D. Lim, S. Park, Metal-free N-doped carbon blacks as excellent electrocatalysts for oxygen reduction reactions, Carbon 145 (2019) 481–487.

[21] F. Yang, X.Y. Ma, W.-B. Cai, P. Song, W.L. Xu, Nature of oxygen-containing groups on carbon for high-efficiency electrocatalytic CO_2 reduction reaction, J. Am. Chem. Soc. 141 (2019) 20451–20459.

[22] L. Lombardi, M. Bandini, Graphene oxide as a mediator in organic synthesis: a mechanistic focus, Angew. Chem. Int. Ed. 59 (2020) 20767–20778.

[23] C.L. Su, M. Acik, K. Takai, J. Lu, S.-J. Hao, Y. Zheng, P.P. Wu, Q.L. Bao, T. Enoki, Y. J. Chabal, K.P. Loh, Probing the catalytic activity of porous graphene oxide and the origin of this behaviour, Nat. Commun. 3 (2012) 1298.

[24] Q.S. Zhang, J.H. Bu, J.D. Wang, C.Y. Sun, D.Y. Zhao, G.Z. Sheng, X.W. Xie, M. Sun, L. Yu, Highly efficient hydrogenation of nitrobenzene to aniline over Pt/CeO_2 catalysts: the shape effect of the support and key role of additional Ce^{3+} sites, ACS Catal. 10 (2020) 10350–10363.

[25] S.U. Dighe, F. Juliá, A. Luridiana, J.J. Douglas, D. Leonori, A photochemical dehydrogenative strategy for aniline synthesis, Nature 584 (2020) 75–81.

[26] W.K. Li, M. Huang, J.H. Liu, Y.-L. Huang, X.-B. Lan, Z.R. Ye, C.Y. Zhao, Y. Liu, Z. F. Ke, Enhanced hydride donation achieved molybdenum catalyzed direct N-alkylation of anilines or nitroarenes with alcohols: from computational design to experiment, ACS Catal. 11 (2021) 10377–10382.

[27] P. Ryabchuk, T. Leischner, C. Kreyenschulte, A. Spannenberg, K. Junge, M. Beller, Cascade synthesis of pyrroles from nitroarenes with benign reductants using a heterogeneous cobalt catalyst, Angew. Chem. Int. Ed. 59 (2020) 18679–18685.

[28] M. Madasu, C.-F. Hsia, S. Rej, M.H. Huang, Cu_2O Pseudomorphic conversion to Cu crystals for diverse nitroarene reduction, ACS Sustain, Chem. Eng. 6 (2018) 11071–11077.

[29] B.K. Yu, S.C. Zou, H.C. Liu, H.M. Huang, Palladium-catalyzed ring-closing reaction via C−N bond metathesis for rapid construction of saturated N-heterocycles, J. Am. Chem. Soc. 142 (2020) 18341–18345.

[30] S.F. Pang, Y.J. Zhang, Q. Su, F.F. Liu, X. Xie, Z.Y. Duan, F. Zhou, P. Zhang, Y. B. Wang, Superhydrophobic nickel/carbon core–shell nanocomposites for the hydrogen transfer reactions of nitrobenzene and N-heterocycles, Green. Chem. 22 (2020) 1996–2010.

[31] D. Xu, R.R. Liu, J.F. Li, H.C. Zhao, J.T. Ma, Z.P. Dong, Atomically dispersed $Co-N_4$ sites anchored on N-doped carbon for aqueous phase transfer hydrogenation between nitroarenes and saturated N-heterocycles, Appl. Catal. B: Environ. 299 (2021), 120681.

[32] G.D. Wen, J.Y. Diao, S.C. Wu, W.M. Yang, R. Schlögl, D.S. Su, Acid properties of nanocarbons and their application in oxidative dehydrogenation, ACS Catal. 5 (2015) 3600–3608.

[33] C.J. Liao, B. Liu, Q. Chi, Z.H. Zhang, Nitrogen-doped carbon materials for the metal-free reduction of nitro compounds, ACS Appl. Mater. Interfaces 10 (2018) 44421–44429.

[34] R. Al-Gaashani, A. Najjar, Y. Zakaria, S. Mansour, M.A. Atieh, XPS and structural studies of high quality graphene oxide and reduced graphene oxide prepared by different chemical oxidation methods, Ceram. Int. 45 (2019) 14439–14448.

[35] S.S. Shang, P.-P. Chen, L.Y. Wang, Y. Lv, W.-X. Li, S. Gao, Metal-free nitrogen- and boron-codoped mesoporous carbons for primary amides synthesis from primary alcohols via direct oxidative dehydrogenation, ACS Catal. 8 (2018) 9936–9944.

[36] Y.B. Mu, M.S. Han, B.K. Wu, Y.M. Wang, Z.W. Li, J.X. Li, Z. Li, S. Wang, J.Y. Wan, L. Zeng, Nitrogen, oxygen-codoped vertical graphene arrays coated 3D flexible carbon nanofibers with high silicon content as an ultrastable anode for superior lithium storage, Adv. Sci. 9 (2022) 2104685.

[37] Y. Liu, L.J. Cao, J. Luo, Y.Y. Peng, Q. Ji, J.Y. Dai, J. Zhu, X.Q. Liu, Biobased nitrogen- and oxygen-codoped carbon materials for high-performance supercapacitor, ACS Sustain, Chem. Eng. 7 (2019) 2763–2773.

[38] W. Xiong, Z.N. Wang, S.L. He, F. Hao, Y.Z. Yang, Y. Lv, W.B. Zhang, P.L. Liu, H. Luo, Nitrogen-doped carbon nanotubes as a highly active metal-free catalyst for nitrobenzene hydrogenation, Appl. Catal. B: Environ. 260 (2020), 118105.

[39] X.D. Long, Z.L. Li, G. Gao, P. Sun, J. Wang, B.S. Zhang, J. Zhong, Z. Jiang, F.W. Li, Graphitic phosphorus coordinated single Fe atoms for hydrogenative transformations, Nat. Commun. 11 (2020) 4074.

[40] M.L. Hua, J.L. Song, X. Huang, H.L. Fan, T.B. Wu, Q.L. Meng, Z.R. Zhang, B.X. Han, Highly efficient C(CO)–C(alkyl) bond cleavage in ketones to access esters over ultrathin N-doped carbon nanosheets, Chem. Sci. 13 (2022) 5196–5204.

[41] M.L. Hua, J.L. Song, X. Huang, H.Z. Liu, H.L. Fan, W.T. Wang, Z.H. He, Z.T. Liu, B. X. Han, Highly efficient oxidative cyanation of aldehydes to nitriles over Se,S,N-tri-doped hierarchically porous carbon nanosheets, Angew. Chem. Int. Ed. 60 (2021) 21479–21485.

[42] P. Anastas, N. Eghbali, Green chemistry: principles and practice, Chem. Soc. Rev. 39 (2010) 301–312.

[43] L.L. Lin, Y.Z. Ge, H.B. Zhang, M. Wang, D.Q. Xiao, D. Ma, Heterogeneous catalysis in water, JACS Au 1 (2021) 1834–1848.

[44] C.-J. Li, L. Chen, Organic chemistry in water, Chem. Soc. Rev. 35 (2006) 68–82.

[45] T. Kitanosono, K. Masuda, P.Y. Xu, S. Kobayashi, Catalytic organic reactions in water toward sustainable society, Chem. Rev. 118 (2018) 679–746.

[46] P. Serna, A. Corma, Transforming nano metal nonselective particulates into chemoselective catalysts for hydrogenation of substituted nitrobenzenes, ACS Catal. 5 (2015) 7114–7121.

[47] J. Li, Y. Long, Y. Liu, L.L. Zhang, Q.S. Wang, X. Wang, S.Y. Song, H.J. Zhang, Robust synthesis of gold-based multishell structures as plasmonic catalysts for selective hydrogenation of 4-nitrostyrene, Angew. Chem. Int. Ed. 59 (2020) 1103–1107.

[48] Y.Y. Chen, J.S. Qiu, X.K. Wang, J.H. Xiu, Preparation and application of highly dispersed gold nanoparticles supported on silica for catalytic hydrogenation of aromatic nitro compounds, J. Catal. 242 (2006) 227–230.

[49] M. Boronat, P. Concepción, A. Corma, S. González, F. Illas, P. Serna, A molecular mechanism for the chemoselective hydrogenation of substituted nitroaromatics with nanoparticles of gold on TiO_2 Catalysts: A cooperative effect between gold and the support, J. Am. Chem. Soc. 129 (2007) 16230–16237.

[50] J.J. Mao, W.X. Chen, W.M. Sun, Z. Chen, J.J. Pei, D.S. He, C.L. Lv, D.S. Wang, Y. D. Li, Rational control of the selectivity of a ruthenium catalyst for hydrogenation of 4-nitrostyrene by strain regulation, Angew. Chem. Int. Ed. 56 (2017) 11971–11975.

[51] W. Liu, H.S. Feng, Y.S. Yang, Y.M. Niu, L. Wang, P. Yin, S. Hong, B.S. Zhang, X. Zhang, M. Wei, Highly-efficient RuNi single-atom alloy catalysts toward chemoselective hydrogenation of nitroarenes, Nat. Commun. 13 (2022) 3188.

[52] J.H. Fu, J.H. Dong, R. Si, K.J. Sun, J.Y. Zhang, M.R. Li, N.N. Yu, B.S. Zhang, M. G. Humphrey, Q. Fu, J.H. Huang, Synergistic effects for enhanced catalysis in a dual single-atom catalyst, ACS Catal. 11 (2021) 1952–1961.

[53] Y. Wang, R.X. Qin, Y.K. Wang, J. Ren, W.T. Zhou, L.Y. Li, J. Ming, W.Y. Zhang, G. Fu, N.F. Zheng, Chemoselective hydrogenation of nitroaromatics at the nanoscale Iron (III)–OH–platinum interface, Angew. Chem. Int. Ed. 59 (2020) 12736–12740.

[54] S. Zhang, C.-R. Chang, Z.-Q. Huang, J. Li, Z.M. Wu, Y.Y. Ma, Z.Y. Zhang, Y. Wang, Y.Q. Qu, High catalytic activity and chemoselectivity of sub-nanometric Pd clusters on porous nanorods of CeO_2 for hydrogenation of nitroarenes, J. Am. Chem. Soc. 138 (2016) 2629–2637.

[55] H.T. Hu, Y.Q. Nie, Y.W. Tao, W.Y. Huang, L. Qi, R.F. Nie, Metal-free carbocatalyst for room temperature acceptorless dehydrogenation of N-heterocycles, Sci. Adv. 8 (2022) 9478.

[56] H.-X. Zhong, Q. Zhang, J. Wang, X.-B. Zhang, X.-L. Wei, Z.-J. Wu, K. Li, F.-L. Meng, D. Bao, J.-M. Yan, Engineering ultrathin C_3N_4 quantum dots on graphene as a metal-free water reduction electrocatalyst, ACS Catal. 8 (2018) 3965–3970.

[57] P. Kumar, E. Vahidzadeh, U.K. Thakur, P. Kar, K.M. Alam, A. Goswami, N. Mahdi, K. Cui, G.M. Bernard, V.K. Michaelis, K. Shankar, C_3N_5: A low bandgap semiconductor containing an azo-linked carbon nitride framework for photocatalytic, photovoltaic and adsorbent applications, J. Am. Chem. Soc. 141 (2019) 5415–5436.

[58] H. Dong, X.T. Guo, C. Yang, Z.Z. Ouyang, Synthesis of $g-C_3N_4$ by different precursors under burning explosion effect and its photocatalytic degradation for tylosin, Appl. Catal. B: Environ. 230 (2018) 65–76.

[59] X.X. Liu, J.Z. Qin, W. Dai, Z.H. Zhu, P. Zhou, Y.X. Wang, J.B. Nie, Y.K. Yang, Z. Z. Zhang, Metal-free and additive-free synthesis of imides and nitriles from ketones via oxidative cleavage of C(O)–C bonds, ACS Catal. 12 (2022) 13300–13311.

[60] X.J. Cui, Z.J. Huang, A.P.V. Muyden, Z.F. Fei, T. Wang, P.J. Dyson, Acceptorless dehydrogenation and hydrogenation of N- and O-containing compounds on $Pd_3Au_1(111)$ facets, Sci. Adv. 6 (2020) 3831.

[61] S. Chakraborty, W.W. Brennessel, W.D. Jones, A Molecular iron catalyst for the acceptorless dehydrogenation and hydrogenation of N-heterocycles, J. Am. Chem. Soc. 136 (2014) 8564–8567.